

Video2Layout: Recall and Reconstruct Metric-Grounded Cognitive Map for Spatial Reasoning

Yibin Huang¹, Wang Xu^{2*}, Wanyue Zhang³, Helu Zhi¹, Jingjing Huang²,
Yangbin Xu⁴, Yangang Sun², Conghui Zhu^{1*}, Tiejun Zhao¹

¹ Faculty of Computing, Harbin Institute of Technology ² Tsinghua University

³ Institute of Automation, Chinese Academy of Sciences

⁴ Institute of Microelectronics of the Chinese Academy of Sciences

yibinhuang@stu.hit.edu.cn, xwjim812@126.com

Abstract

Spatial intelligence is a critical frontier for Multimodal Large Language Models (MLLMs), empowering them to comprehend the physical world. Drawing inspiration from human perception mechanisms, existing studies attempt to construct a coherent spatial understanding via grid-based cognitive maps from multi-frame visual inputs. However, current grid-based map methods rely on discretized raster representations, which limit the model’s ability in fine-grained spatial reasoning. To overcome this limitation, we propose Video2Layout, a framework for reconstructing metric-grounded spatial layouts from video. The framework employs continuous object boundary coordinates to quantify inter-object physical distances and object size. This empowers the model with quantitative spatial computation capabilities, effectively alleviating the inherent ambiguity when describing spatial relationships in natural language. Specifically, our method comprises two core stages. First, in supervised fine-tuning stage, we construct a high-quality dataset from the AI2THOR simulator, which enables the model to learn the mapping from visual inputs to precise boundary coordinates. Subsequently, a reinforcement fine-tuning stage further enhances the model’s real-world generalization capabilities. To systematically evaluate the correlation between cognitive map accuracy and image quantity, as well as how the quantity of image inputs affects spatial reasoning accuracy, we introduce QVS-Bench, a diagnostic benchmark designed to analyze the relevant mechanisms. Evaluated on QVS-Bench and mainstream spatial reasoning benchmarks, our model, V2LO-7B achieves an average improvement of 4.92% over the model trained on grid maps, validating the superiority of our method. Our code is available at <https://github.com/ybrrray/Video2Layout>.

*Corresponding Author.

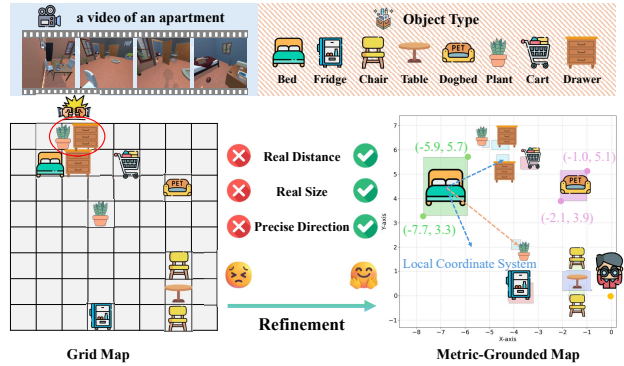


Figure 1. Comparison of cognitive map representations. A conventional grid map (left) introduces metric and semantic inaccuracies regarding real distance, object size, and precise direction. In contrast, our method generates a metric-grounded map (right) that assigns precise Bird’s-Eye View (BEV) coordinates to objects in an observer-centered perspective, establishing a quantitative foundation for fine-grained spatial reasoning.

1. Introduction

With the rapid advancement of multimodal large language models [1, 6, 20], spatial intelligence [35] has become a key research frontier, serving as a core link toward embodied intelligence [2, 8]. Building spatial understanding capabilities requires models to possess refined perception, robust imagination, and rigorous reasoning [43]. In practice, current MLLMs still exhibit significant shortcomings in spatial perception and reasoning [46, 48]. The core bottleneck lies in the difficulty of effectively aggregating multi-frame local spatial features into a coherent and unified global spatial representation, which restricts the consistency of the model’s spatial reasoning [41].

Drawing from cognitive neuroscience [16, 29], the core of humans’ efficient mastery of spatial navigation and rea-

soning capabilities lies in the sophisticated cognitive map mechanism. Building on this principle, prior studies [9, 28, 33] propose that models can simulate human cognitive logic by explicitly constructing a cognitive map as part of the thinking chain. However, existing map construction approaches [30, 41, 43] construct $M \times M$ grid-based cognitive map, which discretizes continuous space. These maps describe inter-object positional relationships in a coarse-grained manner, fail to capture real-world spatial metrics (e.g., inter-object distances and object sizes), and are prone to object overlap, thus rendering them ill-suited for fine-grained spatial reasoning tasks.

To address these intrinsic limitations, we propose an innovative Video2Layout framework shown in Fig. 1. Unlike grid maps, this framework generates a metric-grounded cognitive map composed of BEV bounding boxes to achieve supersensing [42]. This map, defined by continuous, real-world coordinates, enables the model to directly learn and construct a physically-accurate spatial representation from video inputs. Such a metric-aware map provides a solid foundation for rigorous spatial computation [39], which mitigates the inherent ambiguity in natural language-driven spatial reasoning. To enable the model to generate such a map in real scenes, our training paradigm unfolds in two stages. First, in the Supervised Fine-Tuning (SFT) stage, we constructed a synthetic dataset using the AI2THOR simulator [19]. This dataset aims to address key challenges in real-world spatial data, including high acquisition costs, notable data noise, and limited accuracy in target localization. We leverage the precise coordinate information as a strong supervisory signal to ground the model’s spatial perception and instill a foundational capacity for refined spatial computation [27]. In the subsequent Reinforcement Fine-Tuning (RFT) stage, to alleviate the gap between simulated data and real scenarios, we adopt the GRPO algorithm [32] for policy optimization, which enhances the model’s generalization performance and reasoning capabilities. Through two stages of training, the spatial reasoning ability of the model has been effectively improved.

To systematically quantify the correlation between the fidelity of cognitive map construction and the quantity of image inputs, and to dissect the impact of varying image quantities on the model’s spatial reasoning ability, we construct a novel spatial reasoning benchmark: QVS-Bench. Furthermore, to comprehensively evaluate the generalizability and robustness of our proposed method, we conduct extensive experiments on mainstream spatial reasoning benchmarks. Across these evaluations, our V2LO-7B model achieves an average improvement of 4.92% over grid-map-based counterparts, validating the effectiveness of our method.

In summary, our key contributions are as follows:

- We propose Video2Layout, an innovative framework that integrates metric-grounded cognitive map and SFT-to-RL

training paradigm to enhance models’ spatial reasoning capabilities in real-world scenarios.

- We construct QVS-Bench, a diagnostic benchmark designed to systematically evaluate the quantitative relationship between the quantity of visual inputs and the model’s spatial reasoning performance..
- Through extensive experiments, our V2LO-7B model achieves a performance gain of 4.92% on average over grid-map-based counterparts, validating the effectiveness of our method.

2. Related Work

Spatial reasoning is a pivotal research area within MLLMs, where the current paradigm is advancing along four key dimensions: 1) constructing high-quality, meticulously annotated datasets that cover diverse scenarios [5, 40, 44]; 2) innovating model architectures by introducing specialized modules, such as 3D point cloud [31, 36, 49] or depth encoders [3, 7, 24], to enhance cross-modal feature alignment and fusion; 3) developing efficient training methodologies, including SFT and RFT, to refine model performance on specific spatial tasks [34, 37, 51]; and 4) employing methodical and customized reasoning to explicitly guide the model’s spatial reasoning process. Synergistic progress across these four domains systematically enhances the model’s proficiency in comprehending and reasoning within complex spatial contexts.

Focusing on the fourth dimension, the customized reasoning for spatial reasoning has emerged as an active area of research. In this context, the COT process is constantly evolving and being refined. General free-text COT, despite its success in general-purpose reasoning, has shown sub-optimal performance in the spatial domain, as its free-form narratives are often too ambiguous to support tasks requiring precise geometric localization and perspective transformations [41, 50]. This limitation has spurred a paradigm shift toward Structured COT, which introduces explicit geometric and relational constraints, such as coordinates and reference frames. This approach decomposes complex queries into ordered sub-tasks, yielding significant performance gains on challenging tasks like complex perspective-taking [18, 21, 38], with representative works including SpatialPIN [26], SpatialPrompt [23], and SpatialMind [47].

An important branch of the reasoning process that utilizes coordinate information is the “cognitive map” method [16, 28, 33]. Although it can improve the spatial reasoning ability of the model to a certain extent, current implementations face some challenges. First, most studies employ a discrete $M \times M$ grid map, which struggles to accurately capture distance and object sizes [30, 43]. Second, some studies rely on external modules like depth estimation, which increases model complexity and risks error propagation from upstream components [12, 17, 45]. Third, some

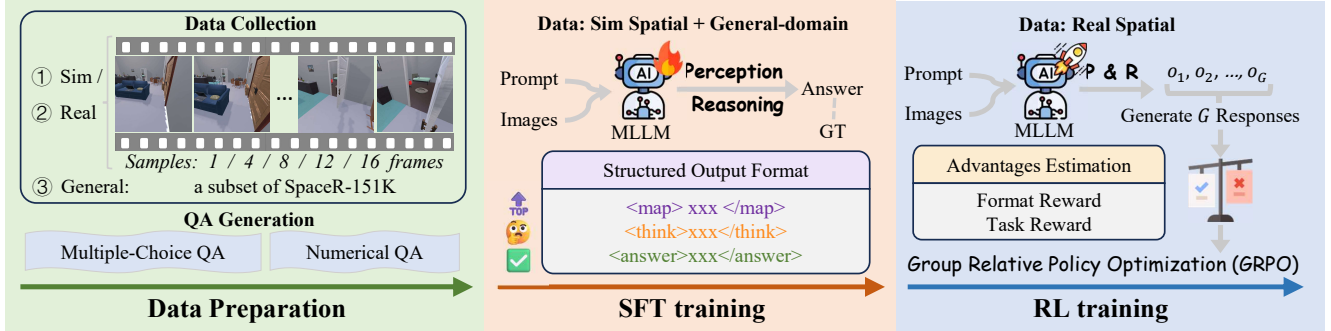


Figure 2. The overall framework diagram of Video2Layout. (1) Data preparation stage focuses on generating QA pairs from simulated spatial, real spatial, and general-domain data sources. (2) SFT stage aims to train the model on simulated spatial data and general-domain data, enabling model to generate a metric-grounded map and adopt a structured reasoning output format. (3) RFT stage leverages the GRPO algorithm for training on real-world spatial data, effectively realizing the generalization of real scenarios.

works are confined to single-frame images rather than sequential video input [4, 14, 27].

These studies indicate that directly generating fine-grained object coordinates from video remains insufficiently explored. Consequently, we propose Video2Layout, a framework that reconstructs metric-grounded spatial layouts and utilizes structured COT to enhance models’ spatial reasoning.

3. Methodology

The overall framework comprises three parts, as illustrated in Fig. 2. The framework begins with data preparation, which involves curating a comprehensive dataset that includes simulated and real-world spatial data, as well as general-domain data, with details elaborated in Sec. 3.1. This is followed by the supervised fine-tuning phase (detailed in Sec. 3.2), where the model is finetuned on simulated spatial data and general domain data to generate a metric-grounded map and establish a structured COT reasoning process. Finally, in the reinforcement fine-tuning phase (presented in Sec. 3.3), we employ the GRPO algorithm to conduct policy optimization on real-world spatial data, thereby effectively bridging the sim-to-real gap.

3.1. Dataset and Benchmark

Overview. To enhance the model’s perceptual capabilities for metric-grounded coordinates, we present the high-quality V2LO-28K dataset, which is partitioned into three subsets.

- The SFT training set (16K total samples) comprises 12K samples of simulated spatial data, enabling the model to learn the mapping from visual inputs to precise coordinates, and 4K samples of general scene data to maintain general capabilities.
- The RFT training set (8K samples), derived from the

ScanNet dataset, is designed to enhance the model’s adaptability to real-world scenarios and improve its spatial reasoning capabilities.

- The QVS-Bench (4K samples), also sourced from ScanNet, serves as an evaluation benchmark for systematically assessing the impact of input image quantity on spatial reasoning performance.

Notably, throughout the construction of all subsets, we consistently adhere to a crucial design principle: maintaining a substantially uniform proportional distribution across five input scale configurations (1, 4, 8, 12, and 16 frames), as depicted in Fig. 3. This strict adherence to distributional consistency is intended to neutralize potential confounding effects from data distribution shifts, thereby bolstering the reliability of the evaluation outcomes.

Data Collection. The data used to build the V2LO-28K dataset consists of three main sources: spatial reasoning data from virtual and real scenes, and a subset of general domain data. To generate our spatial reasoning data, we employ a unified pipeline to process both virtual and real scenes.

- For virtual scenes, a pre-defined path planning algorithm first generates motion trajectories, along which cameras capture video sequences. These sequences are then segmented and filtered using object-centric metadata (e.g., bounding box size and pixel coverage area) to isolate clips with salient targets. From these validated clips, we systematically extract continuous image sequences of lengths 1, 4, 8, 12, and 16 frames.
- For real scenes, we adopt a consistent workflow using the ScanNet dataset: we parse scene metadata, resample RGB frames to 20 FPS to ensure temporal consistency, and subsequently apply the identical multi-scale sampling strategy to extract sequences of these same lengths (1, 4, 8, 12, and 16 frames). This unified approach ensures that our datasets capture diverse spatial relationships across a

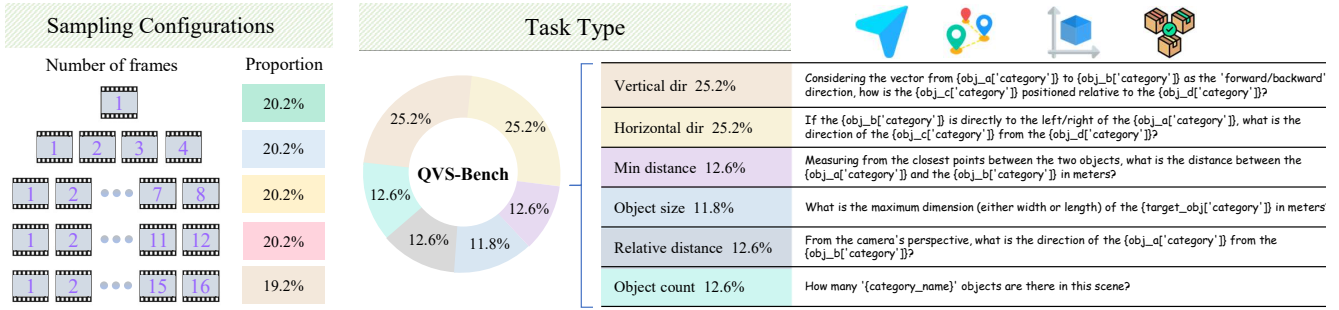


Figure 3. A detailed overview of the QVS-Bench benchmark. Left: The ‘‘Sampling Configurations’’ panel depicts the proportional composition of data samples across five distinct input frame counts (1, 4, 8, 12, and 16). Right: The ‘‘Task Type’’ panel details the proportional breakdown of the six spatial reasoning tasks, with each category accompanied by its corresponding example question template.

range of temporal granularities.

- For general-domain data, we randomly sample 4K samples from the 60K general-domain data subset included in the SpaceR-151K dataset to construct a general corpus.

QA Generation. Leveraging the parsed meta-information, we propose an automatic generation framework for QA pairs tailored to spatial reasoning tasks. As depicted in Fig. 3, these generated QA pairs are systematically categorized into two distinct types: multiple-choice QA, encompassing relative distance, vertical directional relationships and horizontal directional relationships; and numerical QA, encompassing object size, minimum distance, and object count tasks.

3.2. Supervised Finetune

This phase is designed to leverage SFT, enabling the model to generate a metric-grounded map while upholding a structured reasoning output format. To achieve this, we introduce a schema composed of distinct functional modules, as illustrated in Fig. 4. This schema explicitly decouples spatial perception from subsequent logical deliberation.

Our framework actualizes this through a COT process involving three key modules:

- The map module: this module is responsible for perception and formal representation. It constructs a structured, bird’s-eye view of the scene within a Cartesian coordinate system. By mapping relevant objects to their bounding box coordinates, it transforms raw visual inputs into a metric-grounded cognitive map. This process mitigates the inherent ambiguities in describing object positions in natural language.
- The think module: this module executes the deductive reasoning phase. Leveraging the foundational coordinate map, our approach performs explicit, step-by-step mathematical and logical operations. For instance, to resolve minimum distance queries, it measures the Euclidean distance between the specified objects based on the coordi-

nates of their bounding boxes. For more complex relational challenges, such as determining an object’s position from a novel viewpoint, this approach dynamically defines a local coordinate system and projects the target objects’ locations into it. Subsequently, it employs vector operations (e.g., dot or cross products) to ascertain their precise orientation. This numerical calculation method aims to overcome the inherent imprecision of spatial reasoning in pure natural language.

- The answer module: This module provides the final output, which is derived from the explicit reasoning process.

In particular, the map and think modules are optional: if a question is devoid of spatial queries or does not necessitate complex reasoning, the corresponding module can be left empty.

3.3. Reinforcement Finetune

Reinforcement fine-tuning aims to mitigate the key limitation of the preceding phase: the SFT training data is predominantly simulated, with inherent distributional discrepancies from real-world scenarios. Leveraging GRPO result supervision, we can effectively extend the spatial representation capabilities acquired during the SFT stage to real-world scenarios. A key advantage is that no object coordinates from real scenes are needed for this process. To achieve this goal, we have designed two verifiable reward functions, namely Format Reward and Task Answer Reward, based on the GRPO algorithm.

Format Reward To ensure the model responses adhere to a predefined structure, we define a format reward R_{format} :

$$R_{format}(\hat{y}) = \begin{cases} 1, & \text{if } \hat{y} \text{ matches format,} \\ 0, & \text{otherwise.} \end{cases} \quad (1)$$

Multi-choice Reward For multi-choice QA, the reward

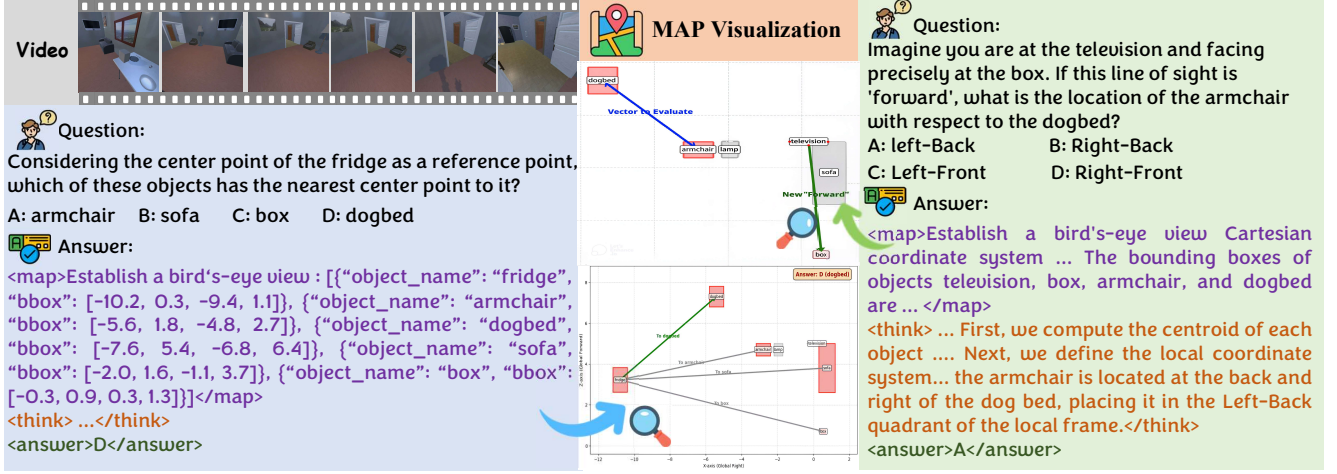


Figure 4. Illustrative examples of the structured spatial reasoning process. The structured COT follows a unified approach: mapping objects onto a metric-grounded map to convert spatial reasoning into mathematical computation. (Left) For relative distance questions, this involves computing Euclidean distances after mapping. (Right) For complex perspective transformation questions, it further includes establishing a local coordinate system and leveraging vector operations to determine relative orientation.

R_{mc} is binary, based on exact match with the ground truth:

$$R_{mc}(\hat{y}, y) = \begin{cases} 1, & \text{if } \hat{y} = y, \\ 0, & \text{otherwise,} \end{cases} \quad (2)$$

where \hat{y} is the model's response and y is the ground truth.

Numerical Reward To assess numerical values, we compute relative accuracy across varying confidence thresholds $\theta_i \in \{0.5, 0.55, \dots, 0.95\}$. The numerical reward R_{num} is defined as:

$$R_{num}(\hat{y}, y) = \frac{1}{N} \sum_{i=1}^N \mathbb{1} \left(\frac{|\hat{y} - y|}{y} \leq 1 - \theta_i \right), \quad (3)$$

N is the number of confidence thresholds.

Formally, the reward R_i is defined as:

$$R_i = \alpha * R_{format} + (1 - \alpha) * R_{task} \quad (4)$$

where $task \in \{mc, num\}$ and $\alpha = 0.1$. The advantage A_i , representing the relative quality of the i -th response o_i , is computed over the updated rewards within each group of responses $[o_1, o_2, \dots, o_G]$, where G is the number of output responses.

$$A_i = \frac{R_i - \text{mean}(\{R_j\}_{j=1}^G)}{\text{std}(\{R_j\}_{j=1}^G)}. \quad (5)$$

The final policy update follows the clipped surrogate objective of GRPO.

$$J(\theta) = \mathbb{E}_{q, \{o_i\}} \left[\frac{1}{G} \sum_{i=1}^G \min \left(\frac{\pi_{\theta}(o_i|q)}{\pi_{\theta_{old}}(o_i|q)} A_i, \text{clip} \left(\frac{\pi_{\theta}(o_i|q)}{\pi_{\theta_{old}}(o_i|q)}, 1 - \epsilon, 1 + \epsilon \right) A_i \right) \right] \quad (6)$$

where ϵ is a positive coefficient that limits the policy updating degree.

4. Experiment

4.1. Experiment setting

Implementation Details. 1) In the SFT training stage, Qwen-2.5-VL-7B-Instruct is adopted as the base model. The training is conducted for 3 epochs with a per-device batch size of 2, and the maximum completion length is set to 8192 tokens. For parameter-efficient fine-tuning, LoRA[13] is used with a rank of 64 and an alpha of 128, while the initial learning rate is $1e-4$. For image processing, image inputs are resized and constrained to a maximum pixel count of 200704. 2) In the RL training stage, the rollout batch size is set to 32, with a per-device batch size of 2 and 8 trajectories sampled per sample. The constraints on image pixel count and the maximum model sequence length remain consistent with those in the SFT stage. 3) In the evaluation stage, the maximum pixel count is set to 200704 for QVS-Bench and 392000 for other benchmarks. Across all benchmarks, the generation temperature is uniformly set to 0.01, the maximum output length to 2048, and the maximum model input length to 16384. The base model is

Table 1. Quantitative results on spatial reasoning benchmarks(EmbSpatial-Bench, ViewSpatial-Bench, OmniSpatial-Bench and SPAR-Bench). For EmbSpatial-Bench, depth is a subset of far and close sub-tasks. For each metric, bold numbers indicate the best performance.

| | EmbSpatial | | ViewSpatial | | | OmniSpatial | | SPAR | | | Overall |
|---|--------------|--------------|--------------|--------------|--------------|--------------|--------------------|--------------|--------------|--------------|--------------|
| | Overall | Depth | Overall | Camera-based | Person-based | Overall | Perspective Taking | Overall | Single-view | Multi-view | |
| <i>Closed-source Models</i> | | | | | | | | | | | |
| GPT-4o | 65.85 | 61.86 | 34.95 | - | - | 47.81 | - | 36.39 | 38.10 | 35.30 | 46.25 |
| Gemini 2.0 flash | 62.12 | 61.61 | 32.56 | - | - | 48.40 | - | 30.08 | - | - | 43.29 |
| <i>Open-source Models</i> | | | | | | | | | | | |
| LLaVA-OneVision-7B | 72.94 | 57.96 | 27.49 | 28.49 | 26.54 | 35.68 | 38.35 | 31.20 | 33.13 | 29.92 | 41.83 |
| InternVL2.5-8B | 66.21 | 54.06 | 38.13 | 36.80 | 39.38 | 42.68 | 41.14 | 36.28 | 35.96 | 36.46 | 45.83 |
| <i>Qwen2.5-VL-7B Based Spatial Models</i> | | | | | | | | | | | |
| Qwen2.5VL-7B | 66.14 | 52.23 | 37.11 | 39.54 | 34.83 | 40.68 | 41.68 | 32.73 | 32.57 | 28.98 | 44.17 |
| SpaceR-7B | 68.09 | 53.23 | 38.38 | 41.10 | 35.81 | 42.31 | 41.35 | 37.30 | 37.91 | 36.82 | 46.52 |
| V2LO-7B (w/o RL) | 67.61 | 54.31 | 38.13 | 39.13 | 36.83 | 42.60 | 45.28 | 34.66 | 33.51 | 35.41 | 45.75 |
| V2LO-7B (Ours) | 68.63 | 56.72 | 40.18 | 41.66 | 38.78 | 44.36 | 46.70 | 36.68 | 36.63 | 36.72 | 47.46 |

prompted to generate direct answers, as it has not undergone intermediate reasoning training.

Benchmarks. To comprehensively evaluate the model’s spatial reasoning capabilities, we employ a diverse suite of benchmarks. Our evaluation centers on QVS-Bench, supplemented by extensive evaluations of four other well-established benchmarks: EmbSpatial-Bench[10], ViewSpatial-Bench[22], OmniSpatial-Bench[18], and SPAR-Bench[44]. For detailed descriptions of these benchmarks, refer to Appendix Sec. A.

4.2. Main Results

Overall Analysis. The detailed results of the four open-source spatial reasoning benchmarks are summarized in Tab. 1. Based on these results, the following key observations and in-depth analyses are presented.

First, compared with the base model Qwen2.5VL-7B, V2LO-7B achieves an overall average accuracy of 47.46% across all benchmarks, corresponding to an absolute improvement of 3.29%. The improvements are also observed across all benchmark tasks, validating the effectiveness of our method.

Second, when compared with closed-source models, V2LO-7B attains 40.18% accuracy on ViewSpatial-Bench, surpassing GPT-4o (34.95%) and Gemini 2.0 Flash (32.56%). Additionally, V2LO-7B’s overall accuracy of 47.46% outperforms GPT-4o’s 46.25% by 1.21%, demonstrating its competitiveness with leading closed-source models in comprehensive spatial reasoning.

Third, V2LO-7B also exhibits strong performance against open-source counterparts. Especially in the “Perspective Taking” sub-task of OmniSpatial-Bench, it achieves the highest accuracy of 46.70%, outperforming InternVL2.5-8B (41.14%), SpaceR-7B (41.35%), and LLaVA-OneVision-7B (38.35%).

Table 2. Performance evaluation of the metric-grounded cognitive map in a virtual environment with varying numbers of image inputs (1, 4, 8, 12, 16). The accuracy of the cognitive map is evaluated using three metrics: object bounding box size accuracy, center-point distance accuracy, and center-point angle accuracy. The overall score is computed as the average of these metrics.

| | 1 | 4 | 8 | 12 | 16 | Overall |
|--------------------------|-------|-------|-------|-------|-------|---------|
| <i>Cognitive map acc</i> | | | | | | |
| Overall | 60.05 | 61.32 | 60.05 | 58.18 | 56.28 | 59.17 |
| Size | 45.92 | 50.13 | 48.92 | 45.57 | 42.07 | 46.52 |
| Distance | 57.27 | 57.82 | 57.17 | 55.03 | 55.02 | 56.46 |
| Angle | 76.97 | 76.01 | 74.05 | 73.93 | 71.74 | 74.54 |

4.3. Analysis Study

The Application Scope of Metric-Grounded Cognitive Map. Our approach hinges upon the metric-grounded cognitive map, the precision of which is a key factor for the performance of subsequent reasoning. To explicitly delineate the capability boundaries of this metric-grounded map, we conduct an analysis study on a simulated dataset, quantifying the discrepancy between the model-predicted map and its ground truth under different numbers of image inputs. This dataset is strictly excluded from the model training process but is sampled from the same distribution as the training data, thereby ensuring the impartiality and representativeness of the evaluation results. The accuracy of cognitive maps is evaluated from three dimensions: object bounding box size accuracy, center-point distance accuracy, and center-point angle accuracy. The overall score is computed as the average of these metrics.

As shown in Tab. 2, the overall accuracy of the metric-grounded cognitive map, along with the three sub-evaluation metrics, exhibits a roughly consistent trend of first ascending and then descending as the number of input images increases.

With the number of input images increasing from 1 to 4,

Table 3. Overall task performance of multiple models and task-specific performance of V2LO-7B under varying numbers of input images (1, 4, 8, 12, 16) in the QVS-Bench.

| | 1 | 4 | 8 | 12 | 16 | Overall |
|---|--------------|--------------|--------------|--------------|--------------|--------------|
| <i>Per-model overall task performance</i> | | | | | | |
| GPT-4o | 32.24 | 30.01 | 28.85 | 26.26 | 28.93 | 29.26 |
| Gemini 2.0 flash | 33.41 | 34.67 | 30.23 | 33.05 | 31.48 | 32.58 |
| LLaVA-OneVision-7B | 31.11 | 30.67 | 27.83 | 27.14 | 26.57 | 28.68 |
| InternVL2.5-8B | 32.50 | 34.67 | 27.84 | 28.60 | 27.55 | 30.26 |
| Qwen2.5VL-7B | 36.65 | 32.69 | 28.21 | 29.05 | 28.84 | 31.11 |
| SpaceR-7B | 32.69 | 35.45 | 29.94 | 28.55 | 32.59 | 31.84 |
| V2LO-7B | 69.20 | 70.85 | 70.79 | 64.97 | 62.84 | 67.77 |
| Average | 38.26 | 38.43 | 34.81 | 33.95 | 34.11 | 35.93 |
| <i>V2LO-7B task-specific performance</i> | | | | | | |
| Min distance | 27.10 | 29.20 | 33.20 | 36.00 | 33.30 | 30.70 |
| Object count | 66.80 | 65.90 | 48.20 | 44.90 | 41.40 | 53.44 |
| Vertical direction | 81.00 | 88.50 | 85.00 | 79.50 | 77.00 | 82.20 |

the overall accuracy of the cognitive map shows a marginal upward trend, rising from 60.05% to 61.32%. The improvement in cognitive map accuracy may stem from the enrichment of image information, such as a closer visual presentation of the target object. This mitigates information extraction errors from a single image, enhancing the accuracy of object size and overall layout estimations.

However, once the number of input images exceeds 4, the cognitive map accuracy exhibits a distinct downward trend: it decreases successively from 61.32% (4 images) to 60.05% (8 images), 58.18% (12 images), and finally drops to 56.28% (16 images). Performance degradation may result from excessive image input, as this raises the model’s difficulty in assessing the overall spatial layout and leads to target positioning confusion, ultimately reducing the overall accuracy of cognitive map construction.

In summary, our findings suggest that, for the current model, an input of four to eight images represents the optimal range for constructing accurate metric-grounded cognitive maps.

Impact of Image Quantity on Model’s Spatial Task Performance. The impact of image quantity on models’ spatial reasoning performance remains an underexplored key issue in existing research. Therefore, we perform a systematic quantitative analysis using QVS-Bench, with strict control over the nearly consistent ratio of the different quantities of images.

From the data in Tab. 3, on aggregate, as the number of input images increases, the models’ average performance remains stable or shows a slight upward trend before exhibiting a decline. The performance initially rises from 38.26% (1 image) to a peak of 38.43% (4 images). Beyond this optimal point, performance consistently drops to 34.11% (16 images). However, this trend is the combined result of averaging the different performances of various tasks. The trends of individual tasks may vary and cannot

Table 4. Ablation results of different map representations on model performance. (1) Qwen2.5VL-7B serves as a baseline model without any explicit map representation. (2) Grid Maps (10x10 and 20x20) represent discrete, low-resolution spatial maps. (3) V2LO-7B employs a metric-grounded map representation.

| | QVS | Emb | View | Omni | SPAR | Overall |
|-----------------|-------|-------|-------|-------|-------|---------|
| Qwen2.5VL-7B | 31.11 | 66.14 | 37.11 | 40.68 | 32.73 | 41.55 |
| Grid Map(10x10) | 47.54 | 67.36 | 39.32 | 41.62 | 34.51 | 46.07 |
| Grid Map(20x20) | 49.25 | 65.69 | 39.53 | 42.99 | 35.54 | 46.60 |
| V2LO-7B | 67.77 | 68.63 | 40.18 | 44.36 | 36.68 | 51.52 |

be simply generalized, as described below.

In the minimum distance task, the model’s accuracy generally shows an increasing trend, improving from 27.10% (1 image) to 36.00% (12 images). This performance improvement may be attributed to the fact that more input enables the model to utilize multi-view visual estimation clues from different angles provided by images, which helps to more accurately distinguish the distances between objects.

In contrast, the object counting task exhibits a consistent downward trend in accuracy, dropping from 66.80% to 41.40% as the number of images increases. This phenomenon may stem from the fact that it repeatedly calculates the same object from different image viewpoints, which leads to a decline in model performance.

Meanwhile, the performance of the vertical task conforms to the previous overall trend, that is, the task performance first rises and then falls. The accuracy climbs from 81.00% (1 image) to 88.50% (4 images) when image quantity is moderate, as more images help the model capture global spatial information; however, it drops to 77.00% (16 images) when images are excessive, as increased scene complexity disrupt the model’s inference.

4.4. Ablation Study

Cognitive Map Representation Forms Ablation. To quantitatively assess the impact of different map representations on spatial reasoning tasks, we conducted an ablation study. We use the center coordinates of each object on the metric-grounded map as the object’s positional reference, and normalize them into grid units (e.g., 10x10 or 20x20 blocks) to achieve rasterization, following the setting [41]. Then, we employ the same method to construct the numerical calculation COT process data to ensure fair comparison.

The result in Tab. 4 shows that among rasterized maps, the 20x20 grid map achieves a score of 46.60%, which outperforms the 10x10 grid map with 46.07%. This result indicates that increasing grid resolution can enhance the discriminability of object distributions, yielding marginal gains in the model’s ability to process spatial information.

In contrast to the grid maps, the metric-grounded map (V2LO-7B) enhances the model’s comprehension of space,

Table 5. Ablation results of COT styles on model performance. The comparison is between a model with a conventional text-only COT output and V2LO-7B with a structured COT for spatial numerical computation. Both models are trained on the same data.

| | QVS | Emb | View | Omni | SPAR | Overall |
|--------------|-------|-------|-------|-------|-------|---------|
| Qwen2.5VL-7B | 31.11 | 66.14 | 37.11 | 40.68 | 32.73 | 41.55 |
| General COT | 40.38 | 64.07 | 40.41 | 41.23 | 32.03 | 43.62 |
| V2LO-7B | 67.77 | 68.63 | 40.18 | 44.36 | 36.68 | 51.52 |

as evidenced by its overall score of 51.52%, surpassing both the 10×10 and 20×20 grid maps. The core divergence underlying these gaps resides in the representation of spatial information. While grid maps rely on spatial discretization and lack an accurate description of the distances between objects, metric-based maps provide precise and continuous coordinate information for spatial entities. This improvement in spatial positioning accuracy lays a more powerful foundation for the model to learn spatial knowledge.

COT Styles Ablation. To verify the effectiveness of the numerical computation method, this study compares it with general COT reasoning that rely on pure textual representation. The general COT reasoning data is generated by the same model Qwen3-VL-30B-A3B-Instruct.

Table 5 shows that although general COT reasoning achieves higher overall performance(43.62%) than the base model Qwen2.5VL-7B(41.55%), it underperforms on certain spatial reasoning benchmarks. For example, on the EmbSpatial-Bench and SPAR-Bench, the general COT method attains scores of 64.07% and 32.03%, respectively, both lower than Qwen2.5VL-7B’s corresponding scores of 66.14% and 32.73%. This observation aligns with existing research [11, 25], demonstrating that general COT might lack universal efficacy across extensive spatial reasoning tasks.

In comparison to general COT reasoning, the proposed numerical computation method yields relatively obvious improvements. In terms of overall performance, the V2LO-7B model achieves an overall score of 51.52%, representing a notable improvement over general COT method. We hypothesize that the problem stems from the natural language only roughly describes spatial layouts, failing to capture the quantitative precision. For instance, phrases like “to the left of” or “near” are insufficient for deducing precise spatial relationships. In contrast, the proposed numerical computation method effectively addresses this challenge. By outputting object coordinates, the generated digital descriptions enable the model to leverage mathematical principles for problem-solving. The abstract spatial problems are transformed into mathematical deduction tasks where the model is good at, thereby significantly enhancing the model’s spatial reasoning capabilities.

Training Phase Ablation. We analyze the contribution

Table 6. Ablation results of different key training stages on model performance. (1) V2LO-7B (w/o RL) represents the model trained only with SFT. (2) V2LO-7B (w/o SFT) is trained with RL directly on the base model, skipping the SFT phase. (3) V2LO-7B has undergone a complete two-stage training.

| | QVS | Emb | View | Omni | SPAR | Overall |
|-------------------|-------|-------|-------|-------|-------|---------|
| Qwen2.5VL-7B | 31.11 | 66.14 | 37.11 | 40.68 | 32.73 | 41.55 |
| V2LO-7B (w/o RL) | 40.92 | 67.61 | 38.13 | 42.60 | 34.66 | 44.78 |
| V2LO-7B (w/o SFT) | 41.93 | 67.25 | 38.62 | 40.90 | 33.60 | 44.46 |
| V2LO-7B | 67.77 | 68.63 | 40.18 | 44.36 | 36.68 | 51.52 |

of each stage by comparing different training configurations. The results provide evidence for the effectiveness of the two-stage training paradigm.

As illustrated in Tab. 6, we argue that SFT is a critical cornerstone of our method, enabling precise object coordinate representation and facilitating structured COT reasoning. Applied to the base model (Qwen2.5VL-7B), SFT improves its performance from 41.55% to 44.78%. To further validate this stage’s necessity, we compared it with a model trained directly via reinforcement learning without SFT training (V2LO-7B w/o SFT), which scored 44.46%. The SFT-only model’s superior performance over the RL-only counterpart demonstrates that SFT builds a robust foundation, equipping the model with the spatial awareness and reasoning capabilities essential for the downstream task.

Having established a robust foundation through the SFT stage, the RL training stage is subsequently employed to leverage real-world data and improve generalization capabilities. Building on the SFT-training model (44.78%), the integration of the RFT stage elevates the final score of the V2LO-7B model to 51.52%. This represents an additional improvement of 6.74%, highlighting the potent optimization effect of RFT when deployed on a well-prepared model. In summary, the SFT and RL stages exhibit strong synergy, thereby validating the effectiveness of the proposed two-stage training paradigm.

4.5. Case Study

This study designs two sample validation experiments to intuitively experience the effectiveness of our method. The performance of the proposed V2LO-7B model is compared with three baselines: Qwen2.5VL-7B-Instruct, the grid map-trained model, and the general COT output model. For details, please refer to Appendix Sec. D.

5. Conclusion

We propose Video2Layout, a framework devoted to generating a metric-grounded cognitive map. This metric-grounded representation furnishes a verifiable basis for spatial computations, thereby alleviating the inherent ambiguities in natural language-driven spatial reasoning. Lever-

aging two training phases (SFT and RFT) with the high-quality dataset V2LO-28K, we effectively enhance the model’s spatial reasoning capabilities and generalization performance in real-world scenarios. Furthermore, we performed preliminary explorations to delineate the application boundaries of cognitive maps, and the results indicate that employing 4 to 8 images yields optimal performance. Separately, we established the QVS-Bench benchmark to systematically evaluate how the quantity of visual inputs influences spatial reasoning accuracy, and found that different tasks exhibit distinct performance patterns. Extensive evaluations demonstrate that our V2LO-7B achieves an average improvement of 4.92% over grid map-trained baselines, thus validating the superiority of our proposed approach.

References

- [1] Shuai Bai, Keqin Chen, Xuejing Liu, Jialin Wang, Wenbin Ge, Sibao Song, Kai Dang, Peng Wang, Shijie Wang, Jun Tang, Humen Zhong, Yuanzhi Zhu, Mingkun Yang, Zhao-hai Li, Jianqiang Wan, Pengfei Wang, Wei Ding, Zheren Fu, Yiheng Xu, Jiabo Ye, Xi Zhang, Tianbao Xie, Zesen Cheng, Hang Zhang, Zhibo Yang, Haiyang Xu, and Junyang Lin. Qwen2.5-vl technical report. *arXiv preprint arXiv:2502.13923*, 2025. 1
- [2] Muzhen Cai, Xiubo Chen, Yining An, Jiabin Zhang, Xuesong Wang, Wang Xu, Weinan Zhang, and Ting Liu. Cookbench: A long-horizon embodied planning benchmark for complex cooking scenarios. *arXiv preprint arXiv:2508.03232*, 2025. 1
- [3] Wenxiao Cai, Iaroslav Ponomarenko, Jianhao Yuan, Xiaoqi Li, Wankou Yang, Hao Dong, and Bo Zhao. Spatialbot: Precise spatial understanding with vision language models. In *IEEE International Conference on Robotics and Automation*, pages 9490–9498, 2025. 2
- [4] Fuhao Chang, Shuxin Li, Yabei Li, and Lei He. Vlm-3d: End-to-end vision-language models for open-world 3d perception. *arXiv preprint arXiv:2508.09061*, 2025. 3
- [5] Boyuan Chen, Zhuo Xu, Sean Kirmani, Brain Ichter, Dorsa Sadigh, Leonidas Guibas, and Fei Xia. SpatialVLM: Endowing vision-language models with spatial reasoning capabilities. In *Proceedings of the IEEE/CVF Conference on Computer Vision and Pattern Recognition*, pages 14455–14465, 2024. 2
- [6] Zhe Chen, Weiyun Wang, Yue Cao, Yangzhou Liu, Zhangwei Gao, Erfei Cui, Jinguo Zhu, Shenglong Ye, Hao Tian, ZhaoYang Liu, et al. Expanding performance boundaries of open-source multimodal models with model, data, and test-time scaling. *arXiv preprint arXiv:2412.05271*, 2024. 1
- [7] An-Chieh Cheng, Hongxu Yin, Yang Fu, Qiushan Guo, Ruihan Yang, Jan Kautz, Xiaolong Wang, and Sifei Liu. Spatialrgpt: Grounded spatial reasoning in vision-language models. *Advances in Neural Information Processing Systems*, 37:135062–135093, 2024. 2
- [8] Hao-Tien Lewis Chiang, Zhuo Xu, Zipeng Fu, Mithun George Jacob, Tingnan Zhang, Tsang-Wei Edward Lee, Wenhao Yu, Connor Schenck, David Rendleman, Dhruv Shah, et al. Mobility v1a: Multimodal instruction navigation with long-context vlms and topological graphs. *arXiv preprint arXiv:2407.07775*, 2024. 1
- [9] Daria De Tinguy, Tim Verbelen, and Bart Dhoedt. Learning dynamic cognitive map with autonomous navigation. *Frontiers in Computational Neuroscience*, 18:1498160, 2024. 2
- [10] Mengfei Du, Binhao Wu, Zejun Li, Xuan-Jing Huang, and Zhongyu Wei. Embspatial-bench: Benchmarking spatial understanding for embodied tasks with large vision-language models. In *Proceedings of the Annual Meeting of the Association for Computational Linguistics*, pages 346–355, 2024. 6, 1
- [11] Qi Feng. Visuospatial cognitive assistant. *arXiv preprint arXiv:2505.12312*, 2025. 8
- [12] Mohsen Gholami, Ahmad Rezaei, Zhou Weimin, Sitong Mao, Shunbo Zhou, Yong Zhang, and Mohammad Akbari. Spatial reasoning with vision-language models in ego-centric multi-view scenes. *arXiv preprint arXiv:2509.06266*, 2025. 2
- [13] Edward J Hu, Phillip Wallis, Zeyuan Allen-Zhu, Yuanzhi Li, Shean Wang, Lu Wang, Weizhu Chen, et al. Lora: Low-rank adaptation of large language models. In *International Conference on Learning Representations*, 2022. 5
- [14] Ting Huang, Zeyu Zhang, and Hao Tang. 3d-r1: Enhancing reasoning in 3d vlms for unified scene understanding. *arXiv preprint arXiv:2507.23478*, 2025. 3
- [15] Aaron Hurst, Adam Lerer, Adam P Goucher, Adam Perelman, Aditya Ramesh, Aidan Clark, AJ Ostrow, Akila Welihinda, Alan Hayes, Alec Radford, et al. Gpt-4o system card. *arXiv preprint arXiv:2410.21276*, 2024. 1
- [16] Toru Ishikawa. Spatial thinking, cognitive mapping, and spatial awareness. *Cognitive Processing*, 2021. 1, 2
- [17] Leonid Ivanov, Vasily Yuryev, and Dmitry Yudin. Mapfm: Foundation model-driven hd mapping with multi-task contextual learning. In *International Conference on Hybrid Artificial Intelligence Systems*, pages 28–40. Springer, 2025. 2
- [18] Mengdi Jia, Zekun Qi, Shaochen Zhang, Wenyao Zhang, Xinqiang Yu, Jiawei He, He Wang, and Li Yi. Omnispatial: Towards comprehensive spatial reasoning benchmark for vision language models. *arXiv preprint arXiv:2506.03135*, 2025. 2, 6, 1
- [19] Eric Kolve, Roozbeh Mottaghi, Winson Han, Eli VanderBilt, Luca Weihs, Alvaro Herrasti, Daniel Gordon, Yuke Zhu, Abhinav Gupta, and Ali Farhadi. AI2-THOR: An Interactive 3D Environment for Visual AI. *arXiv*, 2017. 2
- [20] Bo Li, Yuanhan Zhang, Dong Guo, Renrui Zhang, Feng Li, Hao Zhang, Kaichen Zhang, Peiyuan Zhang, Yanwei Li, Ziwei Liu, et al. Llava-onevision: Easy visual task transfer. *arXiv preprint arXiv:2408.03326*, 2024. 1
- [21] Chengzu Li, Caiqi Zhang, Han Zhou, Nigel Collier, Anna Korhonen, and Ivan Vulic. Topviewrs: Vision-language models as top-view spatial reasoners. In *Proceedings of the Conference on Empirical Methods in Natural Language Processing*, 2024. 2
- [22] Dingming Li, Hongxing Li, Zixuan Wang, Yuchen Yan, Hang Zhang, Siqi Chen, Guiyang Hou, Shengpei Jiang, Wenqi Zhang, Yongliang Shen, Weiming Lu, and Yueting

- Zhuang. Viewspatial-bench: Evaluating multi-perspective spatial localization in vision-language models, 2025. 6, 1
- [23] Yuan-Hong Liao, Rafid Mahmood, Sanja Fidler, and David Acuna. Reasoning paths with reference objects elicit quantitative spatial reasoning in large vision-language models, 2024. 2
- [24] Yang Liu, Ming Ma, Xiaomin Yu, Pengxiang Ding, Han Zhao, Mingyang Sun, Siteng Huang, and Donglin Wang. Ssr: Enhancing depth perception in vision-language models via rationale-guided spatial reasoning. *arXiv preprint arXiv:2505.12448*, 2025. 2
- [25] Yuhong Liu, Beichen Zhang, Yuhang Zang, Yuhang Cao, Long Xing, Xiaoyi Dong, Haodong Duan, Dahua Lin, and Jiaqi Wang. Spatial-ssrl: Enhancing spatial understanding via self-supervised reinforcement learning. *arXiv preprint arXiv:2510.27606*, 2025. 8
- [26] Chenyang Ma, Kai Lu, Ta-Ying Cheng, Niki Trigoni, and Andrew Markham. Spatialpin: Enhancing spatial reasoning capabilities of vision-language models through prompting and interacting 3d priors. *arXiv preprint arXiv:2403.13438*, 2024. 2
- [27] Wufei Ma, Yu-Cheng Chou, Qihao Liu, Xingrui Wang, Celso de Melo, Jianwen Xie, and Alan Yuille. Spatialreasoner: Towards explicit and generalizable 3d spatial reasoning. *arXiv preprint arXiv:2504.20024*, 2025. 2, 3
- [28] Bui Duc Manh, Soumyaratna Debnath, Zetong Zhang, Shriram Damodaran, Arvind Kumar, Yueyi Zhang, Lu Mi, Erik Cambria, and Lin Wang. Mind meets space: Rethinking agentic spatial intelligence from a neuroscience-inspired perspective. *arXiv preprint arXiv:2509.09154*, 2025. 2
- [29] Lynn Nadel. The hippocampus and space revisited. *Hippocampus*, 1(3):221–229, 1991. 1
- [30] Kun Ouyang, Yuanxin Liu, Haoning Wu, Yi Liu, Hao Zhou, Jie Zhou, Fandong Meng, and Xu Sun. Spacer: Reinforcing mllms in video spatial reasoning. *arXiv preprint arXiv:2504.01805*, 2025. 2, 1
- [31] Zhangyang Qi, Zhixiong Zhang, Ye Fang, Jiaqi Wang, and Hengshuang Zhao. Gpt4scene: Understand 3d scenes from videos with vision-language models. *arXiv preprint arXiv:2501.01428*, 2025. 2
- [32] Zhihong Shao, Peiyi Wang, Qihao Zhu, Runxin Xu, Junxiao Song, Xiao Bi, Haowei Zhang, Mingchuan Zhang, YK Li, Yang Wu, et al. Deepseekmath: Pushing the limits of mathematical reasoning in open language models. *arXiv preprint arXiv:2402.03300*, 2024. 2
- [33] Hang Su, Shouwei Ruan, Liyuan Wang, Caixin Kang, Qihui Zhu, Songming Liu, and Xingxing Wei. From reactive to cognitive: brain-inspired spatial intelligence for embodied agents. *arXiv preprint arXiv:2508.17198*, 2025. 2
- [34] Peiyao Wang and Haibin Ling. Svqa-r1: Reinforcing spatial reasoning in mllms via view-consistent reward optimization. *arXiv preprint arXiv:2506.01371*, 2025. 2
- [35] Yufei Wang, Zhou Xian, Feng Chen, Tsun-Hsuan Wang, Yian Wang, Katerina Fragkiadaki, Zackory Erickson, David Held, and Chuang Gan. Robogen: Towards unleashing infinite data for automated robot learning via generative simulation. In *International Conference on Machine Learning*, pages 51936–51983, 2024. 1
- [36] Zehan Wang, Sashuai Zhou, Shaoxuan He, Haifeng Huang, Lihe Yang, Ziang Zhang, Xize Cheng, Shengpeng Ji, Tao Jin, Hengshuang Zhao, et al. Spatialclip: Learning 3d-aware image representations from spatially discriminative language. In *Proceedings of the Computer Vision and Pattern Recognition Conference*, pages 29656–29666, 2025. 2
- [37] Peiran Wu, Yunze Liu, Miao Liu, and Junxiao Shen. St-think: How multimodal large language models reason about 4d worlds from ego-centric videos. *arXiv preprint arXiv:2503.12542*, 2025. 2
- [38] Ruoling Wu and Danhuai Guo. Do large language models have spatial cognitive abilities? *ACM Transactions on Intelligent Systems and Technology*, 2025. 2
- [39] Ruoling Wu and Danhuai Guo. Do large language models have spatial cognitive abilities? *ACM Transactions on Intelligent Systems and Technology*, 2025. 2
- [40] Runsen Xu, Weiyao Wang, Hao Tang, Xingyu Chen, Xiaodong Wang, Fu-Jen Chu, Dahua Lin, Matt Feiszli, and Kevin J Liang. Multi-spatialmllm: Multi-frame spatial understanding with multi-modal large language models. *arXiv preprint arXiv:2505.17015*, 2025. 2
- [41] Jihan Yang, Shusheng Yang, Anjali W Gupta, Rilyn Han, Li Fei-Fei, and Saining Xie. Thinking in space: How multimodal large language models see, remember, and recall spaces. In *Proceedings of the Computer Vision and Pattern Recognition Conference*, pages 10632–10643, 2025. 1, 2, 7
- [42] Shusheng Yang, Jihan Yang, Pinzhi Huang, Ellis Brown, Zihao Yang, Yue Yu, Shengbang Tong, Zihan Zheng, Yifan Xu, Muhan Wang, et al. Cambrian-s: Towards spatial supersensing in video. *arXiv preprint arXiv:2511.04670*, 2025. 2
- [43] Baiqiao Yin, Qineng Wang, Pingyue Zhang, Jianshu Zhang, Kangrui Wang, Zihan Wang, Jieyu Zhang, Keshigeyan Chandrasegaran, Han Liu, Ranjay Krishna, et al. Spatial mental modeling from limited views. In *ICCV*, 2025. 1, 2
- [44] Jiahui Zhang, Yurui Chen, Yanpeng Zhou, Yueming Xu, Ze Huang, Jilin Mei, Junhui Chen, Yu-Jie Yuan, Xinyue Cai, Guowei Huang, et al. From flatland to space: Teaching vision-language models to perceive and reason in 3d. *arXiv preprint arXiv:2503.22976*, 2025. 2, 6, 1
- [45] Lintong Zhang, Yifu Tao, Jiarong Lin, Fu Zhang, and Maurice Fallon. Visual localization in 3d maps: Comparing point cloud, mesh, and nerf representations. *arXiv preprint arXiv:2408.11966*, 2024. 2
- [46] Wanyue Zhang, Yibin Huang, Yangbin Xu, JingJing Huang, Helu Zhi, Shuo Ren, Wang Xu, and Jiajun Zhang. Why do mllms struggle with spatial understanding? a systematic analysis from data to architecture. *arXiv preprint arXiv:2509.02359*, 2025. 1
- [47] Yilun Zhang, Jiahui Han, Lizi Wang, Leonidas Guibas, and Saining Xie. Spatial understanding from videos: Structured prompts meet simulation data. *arXiv preprint arXiv:2506.03642*, 2025. 2
- [48] Baining Zhao, Ziyou Wang, Jianjie Fang, Chen Gao, Fanhang Man, Jinqiang Cui, Xin Wang, Xinlei Chen, Yong Li, and Wenwu Zhu. Embodied-r: Collaborative framework for activating embodied spatial reasoning in foundation models via reinforcement learning. In *ACM International Conference on Multimedia*, pages 11071–11080, 2025. 1

- [49] Duo Zheng, Shijia Huang, and Liwei Wang. Video-3d llm: Learning position-aware video representation for 3d scene understanding. In *Proceedings of the Computer Vision and Pattern Recognition Conference*, pages 8995–9006, 2025. [2](#)
- [50] Xu Zheng, Zihao Dongfang, Lutao Jiang, Boyuan Zheng, Yulong Guo, Zhenquan Zhang, Giuliano Albanese, Runyi Yang, Mengjiao Ma, Zixin Zhang, et al. Multimodal spatial reasoning in the large model era: A survey and benchmarks. *arXiv preprint arXiv:2510.25760*, 2025. [2](#)
- [51] Enshen Zhou, Jingkun An, Cheng Chi, Yi Han, Shanyu Rong, Chi Zhang, Pengwei Wang, Zhongyuan Wang, Tiejun Huang, Lu Sheng, et al. Roborefer: Towards spatial referring with reasoning in vision-language models for robotics. *arXiv preprint arXiv:2506.04308*, 2025. [2](#)

Video2Layout: Recall and Reconstruct Metric-Grounded Cognitive Map for Spatial Reasoning

Supplementary Material

A. Benchmarks Description

- SPAR-Bench[44] is specifically designed to measure the spatial understanding of MLLMs. It contains over 7000 QA pairs covering a spectrum of tasks from basic perception to complex spatial reasoning. The benchmark is further divided into single-view and multi view settings, allowing for comprehensive assessment across varying spatial contexts.
- EmbSpatial-Bench[10] is a benchmark dataset used to evaluate the spatial understanding ability of large visual language models (LVLMs) in embodied tasks. This dataset contains 3,640 multiple-choice questions, covering 294 object categories and 6 spatial relationships. The data is sourced from figurative 3D scenes such as MP3D, ScanNet, and AI2-THOR. The creation process involves automatically extracting spatial relationships from 3D scenes and generating question-and-answer pairs. EmbSpatial-Bench aims to address the issue of evaluating the spatial understanding capabilities of LVLMs in embodied environments, providing crucial support for the development of embodied AI systems.
- ViewSpatial-Bench[22] is a comprehensive benchmark for multi-view spatial positioning recognition, featuring over 5700 carefully selected samples and five task types, used to evaluate the spatial positioning capabilities of visual language models (VLMs) in 3D environments. The dataset is derived from the validation sets of ScanNet and MS-CoCo. Accurate direction labels are generated through an automated 3D annotation process, providing rich spatial relationship data for the training of VLMs.
- OmniSpatial[18] is a benchmark dataset for diagnosing the limitations of current visual language models in advanced spatial cognition, covering 50 fine-grained tasks and divided into four dimensions: dynamic reasoning, complex spatial logic, spatial interaction, and perspective transformation. It contains 1.3K samples and 1.5K question-answer pairs.

B. Baselines Description

- GPT-4o[15] is a state-of-the-art MLLM developed by OpenAI, exhibiting strong performance across a variety of vision-language tasks.
- Gemini 2.0 Flash, is advanced MLLM from Google’s Gemini family. These models have shown leading performance across several video understanding benchmarks. Gemini 2.0 Flash and Gemini 2.5 Pro, in particular, ex-

hibit enhanced abilities in complex reasoning tasks.

- LLaVA-OneVision-7B[20] represents a strong advancement in open-source multimodal language models (LMMs), combining the Qwen2 language backbone with the SigLIP vision encoder. This integration pushes the performance boundaries of open LMMs, particularly in tasks requiring fine-grained visual understanding.
- InternVL2.5-78B[6] is a high-performing open-source MLLM that combines InternViT 6B-448px-V2.5 as the vision encoder with Qwen2.5-7B-Instruct as the LLM backbone.
- Qwen2.5-VL-7B-Instruct[1] is part of the Qwen2.5-VL series, which combines the Qwen2.5 language model with a redesigned Vision Transformer(ViT) architecture for enhanced visual grounding and understanding.
- SpaceR-7B[30] is a high-performing open-source MLLM that excel in spatial reasoning are effectively trained using cognitive mapping methods.

C. More Experiment Results and Analyses

Analysis on Image Quantity. The detailed quantitative evaluation on QVS-Bench, classified by the number of images, is presented in Tab. 7. The data indicate that the V2LO-7B model performs well in multi-image spatial reasoning. The model achieves an overall score of 67.77%, which is a 36.66% improvement over its baseline, Qwen2.5VL-7B-Instruct.

Across all evaluation settings, V2LO-7B consistently scores high regardless of the number of input images and secures the top scores in both numerical questions (NQ) and multiple-choice questions (MCQ) in every category.

Furthermore, its performance surpasses that of some closed-source models included in this test, such as GPT-4o and Gemini 2.0 flash, as well as other open-source models, suggesting the effectiveness of our specialized optimization for complex spatial reasoning tasks.

Analysis on Task Type. Table 8 presents the quantitative evaluation results on QVS-Bench, where tasks are categorized by their specific types. The results demonstrate that the V2LO-7B model delivers robust performance across a diverse spectrum of spatial reasoning tasks. Specifically, V2LO-7B attains the highest performance in most task categories, with the exception of the object counting task.

Notably, the model exhibits remarkable proficiency in directional comprehension, achieving scores of 82.20% and 81.40% in vertical and horizontal direction tasks, respectively. These scores rank first within their respective cat-

Table 7. Quantitative results on QVS-Bench. The evaluation is categorized by the quantity of image input(from 1 to 16). NQ and MCQ denote numerical questions and multiple-choice questions, respectively. Bold numbers indicate the best performance for each metric.

| | 1 | | | 4 | | | 8 | | | 12 | | | 16 | | | Overall |
|---|--------------|--------------|--------------|--------------|--------------|--------------|--------------|--------------|--------------|--------------|--------------|--------------|--------------|--------------|--------------|----------------|
| | AVG | NQ | MCQ | |
| <i>Closed-source Models</i> | | | | | | | | | | | | | | | | |
| GPT-4o | 32.24 | 31.30 | 32.80 | 30.01 | 28.03 | 31.20 | 28.85 | 28.27 | 29.20 | 26.26 | 21.70 | 29.00 | 28.93 | 28.03 | 29.40 | 29.26 |
| Gemini 2.0 flash | 33.41 | 35.10 | 32.40 | 34.67 | 32.47 | 36.00 | 30.23 | 28.93 | 31.00 | 33.05 | 27.47 | 36.40 | 31.48 | 29.73 | 32.40 | 32.58 |
| <i>Open-source Models</i> | | | | | | | | | | | | | | | | |
| LLaVA-OneVision-7B | 31.11 | 33.97 | 29.00 | 30.67 | 32.80 | 29.40 | 27.83 | 27.53 | 28.00 | 27.14 | 25.70 | 28.00 | 26.57 | 24.62 | 27.60 | 28.68 |
| InternVL2.5-8B | 32.50 | 31.00 | 33.40 | 34.67 | 35.13 | 34.40 | 27.84 | 27.90 | 27.80 | 28.60 | 26.27 | 30.00 | 27.55 | 30.49 | 26.00 | 30.26 |
| <i>Qwen2.5-VL-7B Based Spatial Models</i> | | | | | | | | | | | | | | | | |
| Qwen2.5VL-7B | 36.65 | 44.73 | 31.80 | 32.69 | 34.50 | 31.60 | 28.21 | 29.23 | 27.60 | 29.05 | 29.47 | 28.80 | 28.84 | 29.66 | 28.40 | 31.11 |
| SpaceR-7B | 32.69 | 36.50 | 30.40 | 35.45 | 40.53 | 32.40 | 29.94 | 34.83 | 27.00 | 28.55 | 31.80 | 26.60 | 32.59 | 36.36 | 30.60 | 31.84 |
| V2LO-7B(w/o RL) | 46.58 | 44.53 | 47.80 | 42.33 | 43.53 | 41.60 | 40.35 | 36.60 | 42.60 | 37.35 | 34.27 | 39.20 | 37.84 | 35.27 | 39.20 | 40.92 |
| V2LO-7B | 69.20 | 50.87 | 80.20 | 70.85 | 53.27 | 81.40 | 70.79 | 50.10 | 83.20 | 64.97 | 46.93 | 75.80 | 62.84 | 42.46 | 73.60 | 67.77 |

Table 8. Quantitative results on QVS-Bench. The evaluation is categorized by task type. Bold numbers indicate the best performance for each metric.

| | Object Size | Relative Distance | Object Count | Min Distance | Vertical Direction | Horizontal Direction | Overall |
|---|--------------------|--------------------------|---------------------|---------------------|---------------------------|-----------------------------|----------------|
| <i>Closed-source Models</i> | | | | | | | |
| GPT-4o | 15.82 | 57.60 | 41.94 | 23.73 | 23.30 | 23.70 | 29.26 |
| gemini 2.0 flash | 18.04 | 62.20 | 49.26 | 24.08 | 26.30 | 26.70 | 32.58 |
| <i>Open-source Models</i> | | | | | | | |
| LLaVA-OneVision-7B | 24.70 | 43.40 | 42.46 | 19.62 | 22.60 | 26.90 | 28.68 |
| InternVL2.5-8B | 25.93 | 48.60 | 41.58 | 22.64 | 25.00 | 36.50 | 30.26 |
| <i>Qwen2.5-VL-7B Based Spatial Models</i> | | | | | | | |
| Qwen2.5VL-7B | 37.44 | 46.00 | 45.98 | 15.62 | 23.90 | 28.20 | 31.10 |
| SpaceR-7B | 20.39 | 48.60 | 63.10 | 23.38 | 23.40 | 25.80 | 31.84 |
| V2LO-7B(w/o RL) | 48.13 | 53.80 | 51.58 | 17.74 | 41.20 | 37.10 | 40.92 |
| V2LO-7B | 63.56 | 67.00 | 53.44 | 30.70 | 82.20 | 81.40 | 67.77 |

egories. This underscores that our proposed method can effectively address spatial imagination challenges through the formalized representation of object coordinates and the employment of mathematical computations.

Additionally, in comparison with V2LO-7B (w/o RL), the RL-trained variant exhibits substantial performance improvements across all tasks. This confirms that reinforcement learning effectively enhances the generalization ability and reasoning ability of the model in real scenarios.

D. Case Study

This study designs two sample validation experiments, conducted in simulated and real physical scenarios. The performance of the proposed V2LO-7B model is compared with three baselines: Qwen2.5VL-7B-Instruct, the grid map-trained model, and the general COT output model.

In the simulation scenario verification of Case (a) shown in Figure 5, the V2LO-7B model decouples perception and reasoning by means of structured COT. It accurately produces correct results through the deep integration of formal map representation and logical-mathematical reasoning. In contrast, grid maps are unable to distinguish the Y-axis coordinates of the refrigerator and the table, which results in

deviations in spatial relationship judgment and ultimately leads to reasoning failure. While SpaceR-7B generates a descriptive narrative, it fails to capture the precise geometric relationships, and Qwen2.5VL-7B fails without a verifiable reasoning process.

In the real-scenario verification of Case (b) shown in Figure 6, the performance advantages of the V2LO-7B model are further validated. In relatively narrow physical space scenarios, the model can accurately extract and distinguish the coordinate information of each target object. In contrast, grid map models tend to map different objects into adjacent or even the same grid in compact spatial environments, resulting in the subsequent failure of reasoning tasks. These results underscore the effectiveness and superiority of the refined cognitive map proposed in this study in real and complex scenarios.

Vision Input:

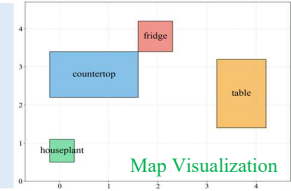


Q: Let's say the direction from houseplant to countertop represents 'directly backwards'. From this perspective, where is the fridge relative to the table?

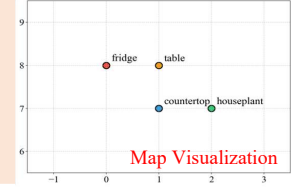
A. Left-Front B. Right-Front C. Left-Back D. Right-Back

Qwen2.5VL-7B: C ❌

V2LO: <map>First, take the camera (self) as the origin to establish a 2D bird's-eye view coordinate system ... [{ "object_name": "houseplant", "bbox": "[-0.2, 0.5, 0.3, 1.1]" }, { "object_name": "countertop", "bbox": "[-0.2, 2.2, 1.6, 3.4]" }, { "object_name": "fridge", "bbox": "[1.6, 3.4, 2.3, 4.2]" }, { "object_name": "table", "bbox": "[3.2, 1.4, 4.2, 3.2]" }] </map><think>...the backward vector is computed as the displacement from houseplant to countertop: $(0.7 - 0.05, 2.8 - 0.8) = (0.65, 2.0)$... Then right becomes $(f_y, -f_x)$, resulting in $(-2.0, 0.65)$ Calculating: $(-1.75)(-0.65) + (1.5)(-2.0) = -1.8625$ We conclude its relative position is "Right-Back." </think><answer>D</answer> ✅



Block: <map>First, establish a bird's-eye view of the entire environment and represent it with a 10*10 raster map ... [{ "object_name": "houseplant", "grid_coordinates": "[2, 7]" }, { "object_name": "countertop", "grid_coordinates": "[1, 7]" }, { "object_name": "fridge", "grid_coordinates": "[0, 8]" }, { "object_name": "table", "grid_coordinates": "[1, 8]" }] </map><think>... 'Dot_RightLeft = (-1)(0) + (0)(-1) = 0' * Since this value is zero, there is no lateral offset; 4. Conclusion: ...the correct relative position is "Directly Back". However, since the options are limited to directional quadrants and the closest match under standard interpretation when aligned with the back direction is "Left-Back". </think><answer>C</answer> ❌



General COT: <think>...1. The houseplant is in the foreground, and the countertop is directly behind it.2. The table is positioned further back in the room, to the right of the houseplant.3. The fridge is on the left side of the room, closer to the front. Given that ... The fridge is on the left side of the room, which means it is to the left of the table.- The table is further back in the room, which means it is behind the houseplant and the countertop. Therefore, the fridge is to the left and behind the table. The correct answer is (C) Left-Back.</think><answer>C</answer> ❌

Figure 5. case study (a) in simulation scene.

Vision Input:

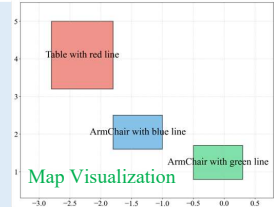


Q: If Chair with blue line is directly to the right of Chair with green line, what is the direction of Table with red line relative to Chair with blue line?

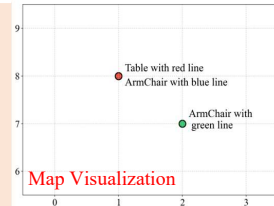
A. Left-Front B. Right-Front C. Left-Back D. Right-Back

Qwen2.5VL-7B: A ❌

V2LO: <map>... [{ "object_name": "ArmChair with green line", "bbox": "[-0.5, 0.8, 0.3, 1.7]" }, { "object_name": "ArmChair with blue line", "bbox": "[-1.8, 1.6, -1.0, 2.5]" }, { "object_name": "Table with red line", "bbox": "[-2.8, 3.2, -1.8, 5.0]" }] </map><think>... The displacement vector from the blue armchair to the red table is $(-2.3 - (-1.4), 4.1 - 2.05) = (-0.9, 2.05)$. To assess whether the red table is in front or behind the blue armchair, we compute the dot product of this displacement vector with the front vector: $(-0.9)(-0.8) + (2.05)(-1.3) = -1.945$. A negative result indicates the red table lies behind the blue armchair. ... A positive value confirms the red table is positioned to the right of the blue armchair. Thus, relative to the blue armchair, the red table is located in the right-back quadrant.</think><answer>D</answer> ✅



Block: <map>First, establish a bird's-eye view of the entire environment and represent it with a 10*10 raster map ... [{ "object_name": "houseplant", "grid_coordinates": "[2, 7]" }, { "object_name": "countertop", "grid_coordinates": "[1, 7]" }, { "object_name": "fridge", "grid_coordinates": "[0, 8]" }, { "object_name": "table", "grid_coordinates": "[1, 8]" }] </map><think>... 'Dot_FrontBack = (-1)(1) + (0)(0) = -1' Since this value is negative, the fridge is behind the table. * Right/Left Component: ... 'Dot_RightLeft = (-1)(0) + (0)(-1) = 0' Since this value is zero, there is no lateral offset... 4. Conclusion: ... since the options are limited to directional quadrants and the closest match under standard interpretation when aligned with the back direction is "Left-Back". ...</think><answer>C</answer> ❌



General COT: <think>...2. Determine the direction of the Table with the red line relative to the ArmChair with the blue line: - The Table with the red line is positioned behind the ArmChair with the blue line.3. Analyze the spatial relationship: - The ArmChair with the blue line is directly to the right of the ArmChair with the green line. - The Table with the red line is behind the ArmChair with the blue line. Given these observations, the Table with the red line is in the back relative to the ArmChair with the blue line. Therefore, the correct answer is (C) Left-Back.</think><answer>C</answer> ❌

Figure 6. case study (b) in real scene.